Ultrafast Wavelength-Dependent Lasing-Time Dynamics in Single ZnO Nanotetrapod and Nanowire Lasers

Jae Kyu Song,[†] Jodi M. Szarko,[†] Stephen R. Leone,*[,†] Shihong Li,[‡] and Yiping Zhao[‡]

Departments of Chemistry and Physics, and Lawrence Berkeley National Laboratory, University of California, Berkeley, California 94720, and Department of Physics and Astronomy, University of Georgia, Athens, Georgia 30602

Received: April 11, 2005; In Final Form: May 25, 2005

The ultrafast lasing dynamics of single zinc oxide nanotetrapods and nanowires are investigated by two-color femtosecond excitation/optical injection spectroscopy. The transient spectral gain induced by time-delayed optical injection pulses (400 nm) is used to investigate the spectrally and temporally resolved lasing properties in a single tetrapod or nanowire laser excited by 267-nm pulses. The lasing output pulse exhibits a faster lasing decay time than the carrier decays due to the superlinear dependence of the lasing on the carrier density. Lasing at the low-energy side of the gain bandwidth (392 nm) has a full width at half maximum (fwhm) for stimulated emission of 1.7 ps. Lasing at 390 nm, the high-energy side of the gain bandwidth, has a fwhm of 2.1 ps for a single example nanowire. The change in lasing dynamics as a function of wavelength is affected by band gap renormalization, since lasing in the electron−hole plasma regime depends not only on the carrier density but also on the band gap shift with carrier density.

I. Introduction

Lasing in single nanowires[1−5] of zinc oxide (ZnO) as well as the films[6] and powders[7] of ZnO is widely investigated, because ZnO is a wide band gap (3.37 eV) semiconductor material suitable for UV/blue optoelectronic applications such as light-emitting diodes and laser diodes. Over the past few years, a variety of novel ZnO nanostructures have been fabricated.[8−11] Only a few lasing studies report the temporal behavior of ZnO nanowire lasers,[3,12] although such studies will help to understand the carrier dynamics in nanostructure lasers. The carrier dynamics can elucidate the nature of the stimulated emission and lasing by studying the relationships between the carrier dynamics and lasing behavior. The optical pulses from microcavity quantum well lasers have also been investigated and short pulse widths; also, high photon densities have been obtained,[13,14] which are important for applications in high-speed optical communications.

There are many important ultrafast experimental techniques used to interrogate the time-resolved dynamics in semiconductor materials. Photoluminescence upconversion studies afford information about the radiative dynamics of excited carriers. Transient absorption experiments probe the carrier dynamics in the ground and excited states by observing ground-state bleaching and excited-state absorption or stimulated emission. However, these methods have not been readily applied to single nanostructured devices because of low signal-to-noise ratios. Because the lasing behaviors depend on the characteristics of individual nanostructures,[2] spatially selective single nanowire studies are crucial to understand the lasing mechanisms and carrier dynamics in single nanostructure lasers. The pump-stimulated emission probe method is a robust way to begin interrogating spatially selective nanostructure lasers.[12] The optical gain induced by external optical injection affords a means to reveal carrier dynamics. When optical injection is introduced as a stimulating pulse, it permits a modification of the lasing carriers, thus altering the gain in nanoscale materials and nanoresonators. The effect of an optical injection pulse on the spectral gain is employed to probe the lasing dynamics. Previously we introduced the basic experimental method and showed that the decay time of the lasing is much more rapid than the overall decay of the carriers.[12] In this article, we report the first wavelength-resolved lasing dynamics of single nanostructure lasing devices using the transient effect of time-delayed optical injection pulses. We study the ultrafast carrier and lasing dynamics simultaneously in order to investigate the wavelength-dependent lasing behavior and its relation to the carrier dynamics. Temporal and spectral maps of the optical gain and depletion are explored under lasing conditions, which reveals characteristics of the wavelength-dependent lasing dynamics that can be compared directly to the carrier dynamics.

II. Experimental Section

A vapor-phase transport process is used to grow ZnO tetrapods by heating Zn powder to 700 °C in a quartz tube furnace with an argon flow of 300 sccm under ambient pressure. X-ray diffraction measurements and scanning electron microscopy (SEM) demonstrate the hexagonal wurtzite structures of the legs in the tetrapods.[9] The shapes and lengths of the tetrapods are characterized by SEM and optical microscopy. The diameters and the lengths of the legs of the tetrapods are in the range of 200−800 nm and 10−30 μm, respectively. The optical image of a single tetrapod is presented in Figure 1a. The tetrapods are sonicated in methanol to isolate individual tetrapods. During sonication, some of the legs of the tetrapods are broken to form nanowires. The mixture of tetrapods and nanowires are drop coated on quartz or glass substrates. Confocal scanning microscopy/spectroscopy is used to study the waveguide lasing effects of the tetrapods with 267-nm pulsed excitation. Emission is

* To whom correspondence should be addressed. E-mail: srl@berkeley.edu.

[†] Departments of Chemistry and Physics, and Lawrence Berkeley National Laboratory, University of California, Berkeley, California 94720.

[‡] Department of Physics and Astronomy, University of Georgia, Athens, Georgia 30602.

10.1021/jp051883p CCC: $30.25 © 2005 American Chemical Society
Published on Web 07/30/2005

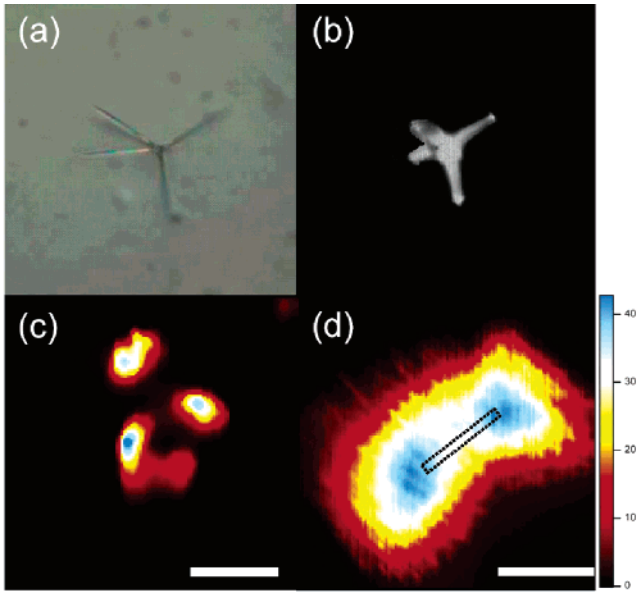

Figure 1. (a) The far-field optical image of a single tetrapod. (b) The far-field emission image induced by 267-nm excitation, which is obtained by collecting UV emissions using a filter. Strong UV emission is observed from each end of the legs of the tetrapod. (c) The confocal scanning image at the lasing wavelength (390 nm) obtained with a scanning piezoelectric stage. Strong emission from the three legs contacted on the substrate is observed. The scale bar is 10 μm. (d) The confocal scanning image of a single nanowire at the lasing wavelength (390 nm). The lasing emission intensity is more distinctive at the end faces than other areas of nanowires. The scale bar is 10 μm.

collected by the microscope objective from a sample on a scanning piezoelectric stage, while the emission wavelength is selected by the monochromator. The spatial resolution used for the confocal imaging is about 1 μm, while the excitation diameter of the 267-nm pulses is about 80 μm for homogeneous excitation.

The details of the apparatus for the ultrafast pump−probe experiments are described elsewhere,[12] and only a brief overview is presented here. An isolated single tetrapod or nanowire is excited by 267-nm pulses and subjected to time-delayed 400-nm probe pulses. The cross correlation between the pump and probe pulse is 300 fs. Both beams are focused onto a single tetrapod or nanowire using a single UV microscope objective, through which the emission as well as the reflected light of the probe is collected. The spectrally resolved light is detected using a photomultiplier tube with a lock-in amplifier. Time-resolved pump−probe experiments are carried out by varying the delay time of the probe pulse with respect to the pump pulse with a variable translation stage, and the intensity of the probe is collected through the monochromator in synchronism with chopping of the pump.

In optical gain spectra, the time-delayed 400-nm pulse is employed as an optical injection pulse rather than a probe, which can be regarded as an external stimulating pulse, since other wavelengths, such as normal lasing wavelengths at 390 nm, are monitored with and without the 400-nm injection pulse. The spectrally resolved optical gain spectra are obtained at the selected delay time of the optical injection. The optical injection beam is chopped, and the integrated emissions with and without the injection pulse are collected as the monochromator is scanned in order to monitor the change in the emissions by the optical injection pulse. The depletion at lasing wavelengths as well as the optical gain at the optical injection wavelength are obtained, which is the spectrally resolved optical gain/depletion spectrum. The time-resolved optical gain spectra are acquired by measuring the emission at selected wavelengths, such as the lasing wavelength, while chopping and varying the delay time of the optical injection pulses with respect to the 267-nm excitation pulses. Therefore the spectral changes induced by the optical injection are investigated as a function of time and wavelength in the lasing nanostructures.

III. Results and Discussion

The waveguide effects of UV photoluminescence (PL) and lasing in ZnO nanowires and nanoribbons have been previously investigated for polarization dependences and spatially resolved emission profiles,[2,3] which showed the efficient coupling of the UV PL and lasing to the nanowaveguides. Lasing is found to be more efficiently coupled to the waveguide through the roundtrips along the lengths of the nanowires. The waveguiding of emissions is also found in tetrapods here, as shown in the far-field emission image of Figure 1b. This image is produced by 267-nm excitation, and only near-UV emissions (360−400 nm) are collected using a filter. The emissions from the ends of each leg are more strongly observed than those from other areas of the tetrapod. Figure 1c shows even clearer waveguiding of the lasing in a tetrapod, through a confocal scanning image obtained at a lasing wavelength of 390 nm by scanning the piezoelectric sample stage. The spatial resolution of the light collection is about 1 μm, while the excitation diameter of the 267-nm beam is about 80 μm. The focal plane of the collected emission is adjusted to be on the substrate. The lasing emission from three legs of the single tetrapod in the plane of the supporting substrate is observed, where the legs are contacted on the substrate. The emission intensity of lasing is similar in each leg. The emission from the fourth leg is not detected, because it is out of the focal plane. When a single leg of the tetrapod is excited, lasing is observed only in that excited leg, and emission is barely detectable from the other legs. When the lasing from the excited leg propagates to other unexcited legs, there will be high losses without amplification for lasing, mainly because of absorption of the lasing,[15,16] scattering losses, and low reflections at the end facet (20%) in the unexcited legs. Therefore, the total gain of lasing during roundtrips along two or more legs can be less than the total loss, which might prevent the lasing through two legs, when only one leg is excited. The results indicate that each leg in the tetrapod can act as an individual nanowire laser. For comparison, the confocal scanning images of single nanowires are also obtained. The lasing emission intensity (390 nm) is more distinctive at the end facets than other areas of the nanowires, as shown Figure 1d, indicating the waveguide nature of the lasing in the nanowires.

An emission spectrum of a nanowire (dotted line) in Figure 2a, isolated by the microscope objective, is obtained with the 267-nm excitation. The excitation intensity of 80 μJ/cm^2 results in a high carrier density in the electron−hole plasma (EHP) regime.[12] In the EHP regime, the band gap is a monotonically decreasing function of increasing carrier density, due to the screening of the Coulomb interaction and exchange and correlation effects,[17−19] which gives rise to the band gap renormalization with a red-shift of emissions.[12] The sharp peaks are assigned to be the longitudinal modes of the lasing, where other emissions such as PL and amplified spontaneous emission contribute to the emission spectrum. Figure 2a also presents the optical gain spectrum[12,20] (solid line) of a given lasing nanowire at the same excitation intensity, which is the change of emissions in the nanowire induced by the optical injection pulse (400 nm, 20 μJ/ cm^2). The optical injection beam is chopped, and the difference of emissions with and without the

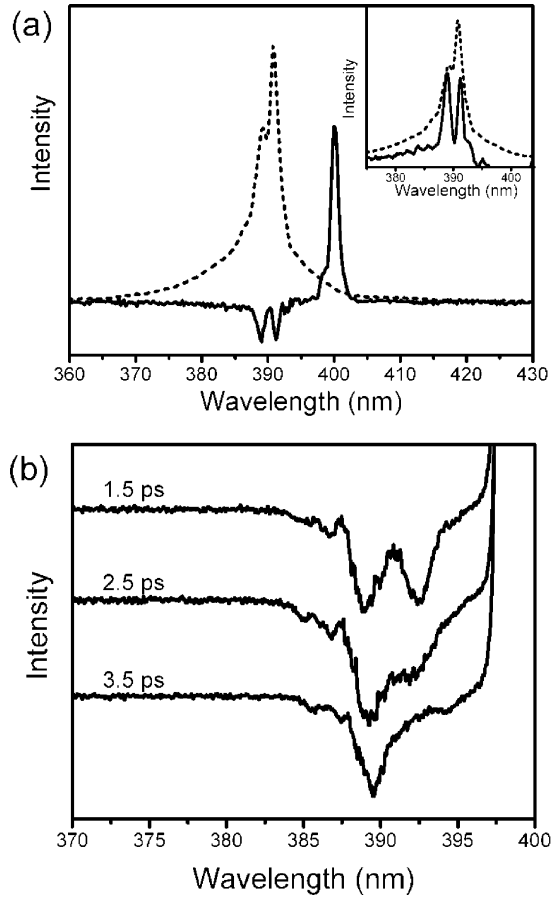

Figure 2. (a) The optical gain spectrum (solid line) obtained with excitation (267 nm) and a time-delayed optical injection pulse (400 nm) at 2 ps and the emission spectrum (dotted line) obtained only with the 267-nm excitation pulse. The inset shows the magnified negative value of the optical gain spectrum. (b) The optical gain spectra at several delay times between the excitation and optical injection pulse.

injection pulse is monitored as the monochromator is scanned. The delay time of the optical injection pulse is 2 ps after the excitation pulse. Two sharp dips are observed along with a much smaller decrease at other wavelengths and a strong increase of emission at the 400 nm optical injection wavelength. The optical injection pulse induces stimulated emission, which depletes the carriers near the band gap edge. The narrow depletion of carriers corresponding to 400 nm is energetically redistributed by carrier−carrier and carrier−phonon scattering processes.[20,21] The original lasing emission at 390 nm decreases dramatically because of the superlinearity of the stimulated emission, even if there is only a small depopulation of the carrier density. To estimate the depopulation, the dependence of the lasing intensity on the excitation intensity is obtained, which is similar to previously reported superlinear dependencies above the lasing or stimulated emission threshold.[5−7,12] The change in the lasing intensity by the optical injection is measured at each lasing mode and compared to the lasing intensities without the optical injection. The depopulation is estimated to be about 3% for this structure at the excitation intensity of 80 μJ/cm^2. For comparison, the time-integrated emission spectrum is presented with the magnified negative value of the optical gain in the inset of Figure 2a. Both the emission and optical gain spectra have peaks at the same wavelengths, proving that the dips correlate with the longitudinal modes of the original 390-nm lasing. We note that the peaks in the optical gain spectrum are narrower than those in the emission spectrum. The lasing modes are more distinct in the optical gain spectrum compared to PL and amplified spontaneous emission because of the superlinear dependence of the lasing on the carrier density.

In addition to the narrow peak shapes, the relative intensities among the longitudinal modes in the optical gain spectrum are different from those in the normal emission and lasing spectrum. To investigate this, several optical gain spectra are obtained as a function of the delay time between the excitation and optical injection pulse. The optical gain spectrum at a delay time of 1.5 ps shows dips at 389 and 392 nm along with the peak at 400 nm, as shown in Figure 2b. As the delay time increases, the depletion at 392 nm smears out, and it is almost absent at a delay time of 3.5 ps. However, the depletion at 389 nm does not change as much. This means that the low-energy side (long wavelength) of the lasing decreases faster than the high-energy side (short wavelength), which is most likely related to the band gap renormalization in the EHP. The amount of band gap renormalization in the EHP is estimated to be about 0.04 eV at this excitation intensity, which agrees with other studies.[17,18,22] The lasing on the low-energy side is accentuated in the reduced band gap of the EHP, which is otherwise below the normal band gap.[17,18] Because the normal band gap is recovered upon the decay of the carrier density,[18] the low-energy side of the lasing in the EHP regime is sustained only in the modified band gap and has a short lasing time. On the other hand, the longitudinal modes on the high-energy side are less affected by the recovery of the band gap, since these are already near the normal band gap and exhibit gain to a degree in the normal band gap over a longer time. The rise time of lasing near the normal band gap is also affected, as discussed below.

Time-resolved pump−probe experiments are carried out to characterize the time scales of EHP decay dynamics, where the 267-nm pump and 400-nm probe intensities are 80 and 20 μJ/cm^2, respectively. The temporal emission stimulated by the probe pulse maps out the carrier density corresponding to the 400-nm probe wavelength (dotted line in Figure 3a). The subpicosecond decrease of the probe observed near zero time is assigned to hot carrier absorption. In a very short rise time of 1 ps, the emission stimulated by the probe pulse is maximized, and there is a biexponential decay with time constants of 3 and 30 ps. The buildup of the EHP is a cooling process from hot carriers to a quasithermalized system with a cooling time of 1 ps, which renormalizes the band gap.[18] After the quasiequilibrium in the EHP, the carrier density decreases by the lasing action, in addition to the normal radiative and nonradiative decays. The rise time (1 ps) and fast decay component (3 ps) of the carrier dynamics obtained by the temporal signal at 400 nm in the lasing nanowire seem to be closely related to the EHP. Therefore, the fast decay component suggests the regime of the EHP dynamics, while the slow decay component is the excitonic dynamics.

Spectral depletion in the optical gain spectrum can be used to probe the lasing dynamics; it shows the relationship between the lasing and carrier dynamics directly. The transient depletion at the normal 392-nm lasing wavelength gives information about the time scale of the lasing dynamics, as the delay time of the optical injection (400 nm) is varied, which is presented as a solid line in Figure 3a. On the other hand, the transient change at a nonlasing wavelength, such as 386 nm (thin line), is hardly noticeable due to the lack of superlinearity in the PL. The rise time of the lasing seems to be closely related to the carrier rise time, which can be compared to the temporal profile of the stimulated emission at 400 nm shown in Figure 3b. The fall time of the lasing pulse seems to be faster than the EHP decay. It is worth noting that lasing times are not identical over the

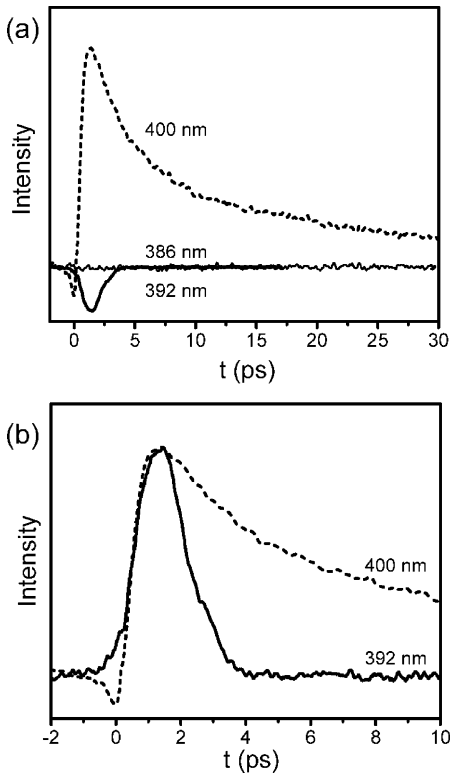

Figure 3. (a) Transient profiles at several wavelengths obtained by time delaying the optical injection pulse (400 nm). At 392 nm (solid line), the temporal profile is primarily characterized by the normal lasing dynamics at this wavelength. (b) Transient depletion profile at 392 nm is negatively normalized in order to compare the profiles between 392 and 400 nm.

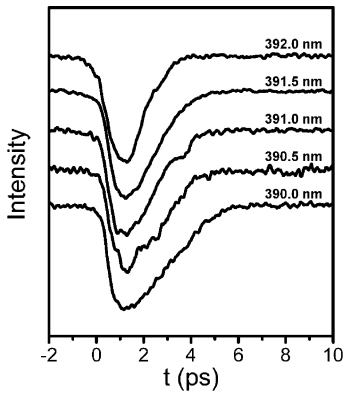

Figure 4. Transient profiles of the lasing dynamics as a function of wavelength from a single nanowire laser. The lasing time becomes longer at shorter lasing wavelengths due to the effect of the band gap shift.

gain bandwidth. The lasing at 392 nm shows the shortest lasing time, as observed in Figure 4. As the lasing wavelength decreases, the lasing time increases, and the longest lasing time is observed at 390 nm. This also suggests that the lasing is affected not only by the carrier density but also by the band gap shift that occurs during the recovery of the normal band gap. The effect of the band gap shift shows the wavelength-dependent lasing dynamics. The lasing time becomes longer at shorter lasing wavelengths (near the normal band gap), since the effect of the band gap shift due to the EHP decay is smaller at those wavelengths.

To understand the temporal profile of the lasing in detail, a rate equation for a semiconductor laser is employed[23]

$$\frac{dP}{dt} = [g(N) - \gamma]P + R_{sp}(N) \quad (1)$$

where P is the photon density, $g(N)$ is the gain, N is the carrier density, γ includes the internal loss and end facet loss, and R_{sp} is the rate of spontaneous emission. For simplicity, the spontaneous emission at the lasing wavelengths is not taken into account, because the intensity of the lasing is much larger than that of the spontaneous emission during the short lasing time. The gain is assumed to be quadratic with the carrier density above the lasing threshold.[5−7,12] The carrier density dynamics are probed by the temporal stimulated emission at 400 nm. If the internal loss and end facet loss do not depend on the carrier and photon density, the best fit is obtained with rise and fall times of 0.8 and 0.9 ps, respectively, for the temporal profile at 392 nm. The transient depletion spectra induced by the optical injection pulse and fitted profiles are shown in Figure 5. The rise time of the lasing in the renormalized band gap is comparable to the cooling time of excited carriers to form the EHP. On the other hand, the lasing at the high-energy side tends to be affected by the recovery of the normal band gap, which also possibly delays the rise time of the lasing. For example, the temporal profile at 390 nm shows relatively slow rise and fall times of 1.1 and 1.2 ps, respectively. As discussed previously, the fall time at 390 nm (near normal band gap) is longer than that at 392 nm (EHP regime), because the high-energy side of the lasing near the normal band gap is less affected by the band gap renormalization, and it is amplified to a degree in the normal band gap for a longer time. However, the fall time of the lasing at 390 nm is still faster than the carrier density decay. This is because of the superlinear dependence of the lasing on the carrier density. The decrease of the carrier density results in a much more dramatic decrease of lasing emission, resulting in a faster decay time of lasing emission. The full width at half maximum (fwhm) of the lasing pulse at 390 nm is 2.1 ps, while the lasing at 392 nm has a pulse duration with a fwhm of 1.7 ps. To our knowledge, this pulse width is the shortest lasing generated from microcavity lasers.[13,14]

A lasing time as long as 9 ps fwhm is observed for some nanowires at an excitation intensity of 80 μJ/cm^2, which also depends on the lasing wavelength, as shown in Figure 6. The differences in lasing times may arise from multiple properties of the nanowires such as the dimensions, end facet quality, defect density, lasing threshold, and substrate coupling. For a single longitudinal mode, the lasing time is given by steady-state approximations for laser diodes[24]

$$\frac{1}{\tau_{ph}} = v_{gr}\left(\alpha + \frac{1}{L}\ln\frac{1}{\sqrt{R_1 R_2}}\right) \quad (2)$$

where v_{gr} is the group velocity, α is the waveguide loss, L is the cavity length, and R is the end facet reflectivity. The optical confinement of lasing in nanowires can affect the waveguide loss. The fractional mode distributions, which are the field intensities retained in the nanowires, are determined largely by the waveguide dimensions.[25−27] As the waveguide diameter becomes comparable to the wavelength, more light is guided outside the wire as an evanescent wave and becomes susceptible to scattering loss due to surface roughness and contamination. Therefore, the waveguide loss will increase with decreasing waveguide diameter.[28] Because the diameter of the nanowires is comparable to the lasing wavelength, the optical confinement will be highly diameter dependent, where the lasing time may change with the nanowire diameters. Nanowires with a long cavity length and well-defined end facets (high reflectivity) can

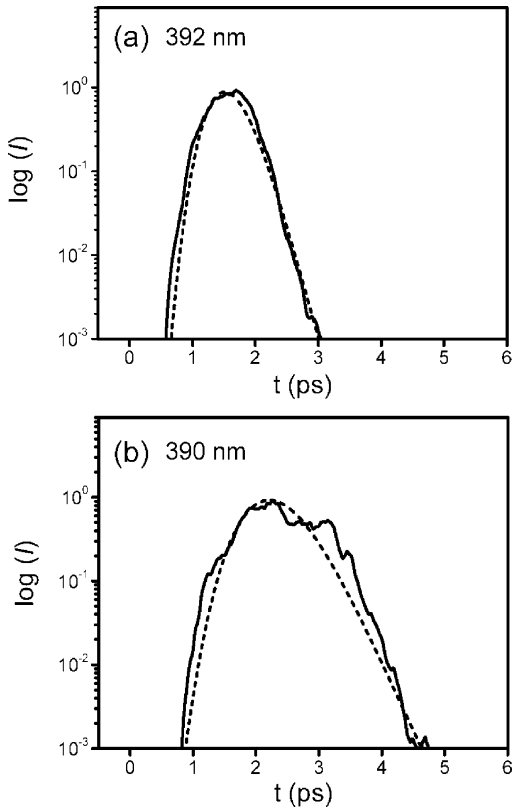

Figure 5. (a) Time evolution of the measured (solid line) and fitted (dotted line) lasing at 392 nm. (b) Time evolution of the measured (solid line) and fitted (dotted line) lasing at 390 nm.

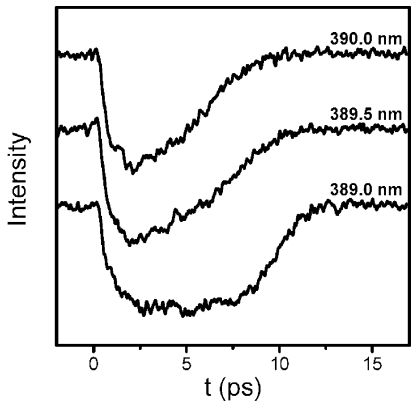

Figure 6. Transient profiles of the lasing dynamics as a function of wavelength from a different single nanowire laser.

sustain lasing longer due to the increase of the optical gain region and a decrease of the loss at the mirrors. The defects can induce a fast decay of emissive carriers to nonemissive states or traps in nanowires with high surface-to-volume ratio,[15] resulting in the fast fall time of lasing.

IV. Conclusions

The ultrafast lasing dynamics of single ZnO tetrapods and nanowires are characterized and compared to the carrier dynamics. The optical gain spectra obtained as a function of time and wavelength provide a means to distinguish the lasing from other emissions and are thus used to investigate the wavelength-dependent lasing dynamics in nanowires for the first time. The fall time of the lasing is faster than the carrier density decay because of the superlinear dependence of the lasing on the carrier density. The lasing at the low-energy side has a faster rise and fall time, while the lasing at the high-energy side shows a slower rise and fall time, which is attributed to the band gap renormalization in the EHP regime and the recovery of the band gap at lower carrier densities. The nanowires show a high photon density lasing pulse as short as a fwhm of 1.7 ps, which depends on the wavelengths and properties of nanowires. We have studied several nanotetrapod and nanowire lasers that show different lasing dynamics due to the intrinsic characteristics of nanostructures such as the dimensions, defect density, and end facet quality. Future studies by controlling each property separately will elucidate more detailed lasing and carrier dynamics in nanostructure lasers for potential applications.

Acknowledgment. The initial lasing experiments were supported by an exploratory grant from the National Science Foundation, ECS-0210106. Construction of the laboratories, additional equipment, and support were provided by the Director, Office of Science, Office of Basic Energy Sciences, Materials Science Division, U.S. Department of Energy under contract No. DE-AC03-76SF00098. The National Institute of Standards and Technology provided some instruments for this work on loan. S.H.L. and Y.P.Z. were supported by the National Science Foundation under Contract No. ECS-0304340.

References and Notes

(1) Huang, M. H.; Mao, S.; Feick, H.; Yan, H.; Wu, Y.; Kind, H.; Weber, E.; Russo, R.; Yang, P. *Science* **2001**, *292*, 1897.

(2) Johnson, J. C.; Yan, H.; Yang, P.; Saykally, R. J. *J. Phys. Chem. B* **2003**, *107*, 8816.

(3) Johnson, J. C.; Knutsen, K. P.; Yan, H.; Law, M.; Zhang, Y.; Yang, P.; Saykally, R. J. *Nano Lett.* **2004**, *4*, 197.

(4) Liu, C.; Zapien, J. A.; Yao, Y.; Meng, X.; Lee, C. S.; Fan, S.; Lifshitz, Y.; Lee, S. T. *Adv. Mater.* **2003**, *15*, 838.

(5) Choy, J.-H.; Jang, E.-S.; Won, J.-H.; Chung, J.-H.; Jang, D.-J.; Kim, Y.-W. *Adv. Mater.* **2003**, *15*, 1911.

(6) Yu, S. F.; Yuen, C.; Lau, S. P.; Lee, H. W. *Appl. Phys. Lett.* **2004**, *84*, 3244.

(7) Cao, H.; Xu, J. Y.; Seelig, E. W.; Chang, R. P. H. *Appl. Phys. Lett.* **2000**, *76*, 2997.

(8) Yan, H.; He, R.; Pham, J.; Yang, P. *Adv. Mater.* **2003**, *15*, 402.

(9) Chen, Z.; Shan, Z.; Cao, M. S.; Lu, L.; Mao, S. X. *Nanotechnology* **2004**, *15*, 365.

(10) Kong, X. Y.; Ding, Y.; Yang, R.; Wang, Z. L. *Science* **2004**, *303*, 1348.

(11) Gao, P. X.; Wang, Z. L. *Appl. Phys. Lett.* **2004**, *84*, 2883.

(12) Szarko, J. M.; Song, J. K.; Blackledge, C. W.; Swart, I.; Leone, S. R.; Li, S.; Zhao, Y. *Chem. Phys.* Lett. **2005**, *404*, 171.

(13) Michler, P.; Lohner, A.; Rühle, W. W.; Reiner, G. *Appl. Phys. Lett.* **1995**, *66*, 1599.

(14) Michler, P.; Hilpert, M.; Rühle, W. W.; Wolf, H. D.; Bernklau, D.; Riechert, H. *Appl. Phys. Lett.* **1996**, *68*, 156.

(15) Egelhaaf, H.-J.; Oelkrug, D. *J. Cryst. Growth* **1996**, *161*, 190.

(16) Muth, J. F.; Kolbas, R. M.; Sharma, A. K.; Oktyabrasky, S.; Narayan, J. *J. Appl. Phys.* **1999**, *85*, 7884.

(17) Bagnall, D. M.; Chen, Y. F.; Zhu, Z.; Yao, T.; Shen, M. Y.; Goto, T. *Appl. Phys. Lett.* **1998**, *73*, 1038.

(18) Takeda, J.; Jinnouchi, H.; Kurita, S.; Chen, Y. F.; Yao, T. *Phys. Status Solidi B* **2002**, *229*, 877.

(19) Klingshirn, C. F. *Semiconductor Optics*; Springer: Berlin, 1997.

(20) de Boer, A. P.; Christianen, P. C. M.; Maan, J. C.; Rasing, Th.; Tolstikhin, V. I.; van de Roer, T. G.; de Vrieze, H. M. *Appl. Phys. Lett.* **1998**, *72*, 2936.

(21) Othonos, A. *J. Appl. Phys.* **1998**, *83*, 1789.

(22) Yamamoto, A.; Kido, T.; Goto, T.; Chen, Y.; Yao, T.; Kasuya, A. *Appl. Phys. Lett.* **1999**, *75*, 469.

(23) Agrawal, G. P.; Gray, G. R. *Appl. Phys. Lett.* **1991**, *59*, 399.

(24) Nakamura, S.; Fasol, G. *The Blue Laser Diode*; Springer: Berlin, 1997.

(25) Snyder, A. W.; Love, D. *Optical Waveguide Theory*; Kluwer: Boston, 1983.

(26) Law, M.; Sirbuly, D. J.; Johnson, J. C.; Goldberger, J.; Saykally, R. J.; Yang, P. *Science* **2004**, *305*, 1269.

(27) Maslov, A. V.; Ning, C. Z. *Appl. Phys. Lett.* **2003**, *83*, 1237.

(28) Tong, L.; Gattass, R. R.; Ashcom, J. B.; He, S.; Lou, J.; Shen, M.; Maxwell, I.; Mazur, E. *Nature* **2003**, *426*, 816.